Elkin L. Romero[1], Mónica Soto-Monsalve[2], Gustavo Gutiérrez[3], Fabio Zuluaga[1], Richard D´Vries[4], Manuel N. Chaur[1*]

[1]Departamento de Química, Facultad de Ciencias Naturales y Exactas. Universidad del Valle.
[2]Instituto de Química de São Carlos. Universidade de São Paulo.
[3]Departamento de Ciencias Farmacéuticas, Facultad de Ciencias Naturales. Universidad Icesi.
[4]Departamento de Ciencias de Ciencias Naturales, Exactas y Estadística. Universidad Santiago de Cali.

***Corresponding author:** manuel.chaur@correounivalle.edu.co

Received: 17/08/17. Accepted: 12/02/18

Structural, spectroscopic, and theoretical analysis of a molecular system based on 2-((2-(4-chlorophenylhydrazone) methyl)quinolone

Abstract

A novel molecular system based on 2-((2-(4-chlorophenylhydrazone)methyl) quinoline (**1-*E***) was synthesized. Interconversion of **1-*E*** to its configurational isomer **1-Z** was achieved using UV radiation (250 W Hg lamp). Such isomerization was monitored by ^{1}H-NMR. The results suggest that the hydrazone derivative can act as a chemical brake in solution. This molecular system was structurally (Single Crystal X-Ray diffraction and DFT calculations) and spectroscopically (NMR, UV, and IR) characterized. Electrochemical measurements showed that configurational changes induce differential redox behavior. In this regard, the reported quinoline system exhibits different dynamic absorption and electrochemical properties that are modulated by UV-light. Therefore, **1-*E*** can be regarded as a potential photo-electrochemical switch.

Keywords: Hydrazone derivatives; configurational dynamic; single XRD; DFT calculations; electrochemistry.

Análisis estructural, espectroscópico y teórico de un sistema molecular basado en la 2-((2-(4-clorofenilhidrazono) metil)quinolina

Resumen

Se sintetizó un nuevo sistema molecular basado en 2-((2-(4-chlorofenilhidrazona) metil)quinolina. Del mismo modo, se evaluó la respuesta dinámica de este compuesto a radiación ultravioleta y formación de un enlace de hidrógeno intramolecular. Los resultados muestran que este derivado de hidrazona puede actuar como freno en solución. El sistema en mención es descrito estructural (Cristalografía de Rayos X y cálculos DFT) y espectroscópicamente (RMN, UV e IR). La interconversión de este sistema entre las configuraciones **1-*E*** y **1-Z** fue mediada por radiación UV y monitoreada a través de RMN-^{1}H. El estudio electroquímico mostró un comportamiento diferencial en función de su configuración, aspecto fundamental en el desarrollo de sistemas foto- y electroquímicamente modulados.

Palabras clave: derivados hidrazónicos; dinámica configuracional; cristalografía de rayos X; cálculos DFT; electroquímica.

Análise estrutural, espectroscópico, e teórico de um sistema molecular com base na 2-((2-(4-Clorofenilhidrazona) metil)quinolina

Resumo

Neste trabalho é apresentado um novo sistema molecular baseado na 2-((2-(4-clorofenilhidrazona)metil)quinolina, capaz de responder dinamicamente à radiação ultravioleta formando uma ligação de hidrogénio intramolecular que atua como um freio na solução. Este sistema é descrito estruturalmente (cristalografia de raios-X e DFT) e por diferentes técnicas espectroscópicas (RMN, de UV e de IV). Radiação UV foi usada para fazer a interconversão da hidrazona **1-*E*** no seu isômero configuracional **1-Z**. Este processo foi monitorado pelo RMN. As medidas eletroquímicas mostraram que as mudanças configuracionais entre os isômeros induzem a comportamentos redox diferentes, o que é uma caraterística chave no desenvolvimento de interruptores fotoelectroquímicos.

Palavras-chave: derivados de hidrazonas; Dinâmica configuracional; Cristalografia de Raios-X; Cálculos DFT; Eletroquímica.

Introduction

The synthesis, characterization, and identification of molecular systems potentially useful in the design of molecular machines is still a huge challenge for supramolecular chemistry researchers (*1, 2*). In this regard, some organic compounds with double bonds (C=C, C=N, or N=N) are of special interest due to their reversible photochemical and thermal reactions. Such feature makes these compounds potentially useful for the synthesis of molecular machines (*3, 4*). It is well known that hydrazone derivatives are one of the most used compounds as building blocks for the formation of supramolecular systems because of the physical and chemical properties that they exhibit. These properties can be reversibly modulated in response to an external stimulus, either light *(5–9)*, addition of metal ions *(10–14)*, and pH changes *(15)*. Hydrazone derivatives based on 2-quinoline are particularly interesting molecules for the development of photo-activated switches as, upon UV-light irradiation, the quinoline-nitrogen may form an intramolecular hydrogen bond with the *N*-H proton from a hydrazine moiety, thus stabilizing the *Z* isomer making even possible to isolate it and study its properties. Additionally, the *E*-isomer can act as a ligand similar to terpydine for metal-ion coordination *(16, 17)*.

Likewise, the study of electronic and electrochemical properties of configurational isomers has not been well documented, at least for hydrazone derivatives, where there are only a few recent reports *(7, 18)*. Electrochemistry of E/Z configurational isomers is important to demonstrate their potential use as molecular photoswitches and electronic devices. Therefore, to design molecular systems able to reversibly modulate the physical and chemical properties in response to light or metal centers, we have decided to study and compare through theoretical studies the electronic and electrochemical properties of the configurational isomers of 2-((2-(4-chlorophenylhydrazono)methyl)-quinoline.

Materials and Methods

All starting reagents were acquired from Sigma-Aldrich (USA) and were used without additional purification. FT-IR, NMR (mono and bi-dimensional), and UV-vis spectra were taken in a Shimadzu FTIR-8400S instrument (Japan), in a 400 MHz Bruker Ultrashield spectrometer (USA), and in a PharmaSpec Shimadzu UV-Vis UV-1700 spectrophotometer (Japan), respectively. Electrochemical measurements were recorded in a bipotentiostat model 700B (USA) series electrochemical Analyzer/Workstation from CH Instruments coupled to a computer.

Synthesis of hydrazone derivatives

The hydrazone derivative (*E*)-2-((2-(4-Chlorophenylhydrazono)methyl) quinoline **1-*E*** was synthesized following the same synthetic protocol as reported in the literature *(7)*. A mixture of 2-methylquinoline (200 mg, 1.40 mmol) and selenium dioxide (263.5 mg, 2.37 mmol) was dissolved in dry dioxane (20 mL). Then, the reaction mixture was heated under reflux and monitored by thin-layer chromatography (TLC). After disappearance of the starting material, a solid was obtained which was filtered and washed with chloroform (3 x 5 mL). The 2-quinolinecarboxaldehyde was purified by column chromatography with a 95:5 $CHCl_3$/MeOH solution getting an 80% yield.

The aldehyde derivative was condensed with 4-chloropehnylhydrazine which was added in a 1:1 ratio in absolute ethanol and heated for 3 h until a red precipitate was formed. This precipitate was washed with cold ethanol and recrystallized from ethanol in 82% yield. Mp 206-208 °C. 205-207 *(19)* ^{1}H NMR (400 MHz, DMSO-d_6) δ 7.34-7.41 (m, 4H), 7.75 (t, 1 H, *J* 7.61), 7.91-8.02 (m, 1 H), 8.16 (d, 1 H, *J* 8.00), 8.25 (d, 1 H, *J* 8.39), 8.33-8.44 (m, 2 H), 8.72 (d, 1 H, *J* 8.98), 12.43 (s, 1 H); ^{13}C NMR (100 MHz, DMSO-d_6) δ 115.8. 118.4, 122.6, 125.9, 126.6, 127.4, 128.4, 128.8, 129.1, 129.7, 133.2, 142.03, 142.8, 152.5.

(Z)-2-((2-(4-chlorophenylhydrazono)methyl)quinoline (1-*Z*)
A solution of 1-*E* in methanol was irradiated with a 250 Watts mercury lamp for 30 min. This compound was purified by column chromatography using $CHCl_3$ as eluent obtaining a yellow oil; yield 65%; ^{1}H NMR (400 MHz, DMSO-d_6) δ 7.22-7.35 (m, 4H), 7.58-7.64 (m, 1H), 7.80 (t, 1H, *J* 7.7 Hz), 7.99-8.05 (m, 2H), 8.11-8.21 (m, 2H), 8.44 (d, 1H, *J* 8.98 Hz), 11.62 (s, 1H).

Single-Crystal structure determination

The data were collected on a Bruker APEX-II CCD diffractometer using MoKα radiation (0.71073 Å) monochromated by graphite at room temperature (296 K). The cell determination and the final cell parameters were acquired on all reflections using the Bruker SAINT software *(20)*, included in APEX2 software suite. Data integration and scaled was carried out using the Bruker SAINT software *(20)*.

The structure was solved using the SHELXS-2013 software and refined using SHELXL-2013 *(21)*, contained in WinGX *(22)*, and Olex2-1.2 *(23)*. Non-hydrogen atoms of the molecules were clearly resolved and full-matrix least-squares refinements of these atoms with anisotropic thermal parameters were performed. All hydrogen atoms were stereochemically positioned and refined with the riding model *(23)*, except for the hydrogen atom bonded to Nitrogen atom, which was found from the density map. ORTEP diagram was generated with Olex^2 *(23)*. Mercury software *(24)* was used to prepare the illustrations.

Electrochemical study of hydrazone derivatives

Cyclic voltammetry (CV) and Osteryoung Square Wave Voltammetry (OSWV) were performed using a 0.1 M solution of tetrabutylammonium hexafluorophosphate ($TBAPF_6$) in DMF. A glassy carbon electrode, a platinum wire, and a silver wire were used as working, counter, and pseudo-reference electrode, respectively. The solutions were degassed with argon before each measurement (10 min). Ferrocene was added as an internal standard. The scan rate was 100 mVs^{-1}.

Computational details

Theoretical calculations were performed using GaussView as graphic interface *(24)* and Gaussian 09 *(26)* for running calculations. Molecular geometry of **1-*E*** in the ground state was optimized by DFT:B3LYP method with 6-311+G (d, p) basis set. NMR chemical shifts were computed at the same level of theory, using the gauge-including atomic orbital (GIAO) method without any solvent or solvation effect considerations.

Vibrational frequencies were performed at the same level than vibrational analysis and assuring that global minima were achieved. Hartree-Fock/6-31+G (d) level of theory and Self-Consistent Isodensity Polarized Continuum Model (SCI-PCM) were employed to simulate solvation effect in optimizations, while UV-Vis spectrum calculations were carried out using same method and level of theory without solvation. For UV-Vis spectrum deconvolution, theoretical IR, and UV spectra graph generation GaussSum 3.0 software package was employed *(27)*.

Results and Discussion

Synthesis and characterization of hydrazone derivatives

Details of the synthesis of **1-*E*** and **1-*Z*** are shown in Figure 1. Compound **1-*E*** was synthesized by the partial oxidation of **2** with selenium dioxide in dioxane, followed by condensation of **3** with the hydrazine derivative **4** in ethanol *(7)*. The condensation reaction led to the formation of the corresponding *E*-hydrazone, which was identified by the singlet at 12.43 ppm corresponding to the NH proton *(3)*. The geometry optimization for **1** was also performed to compare the energy associated to each isomer, as it was expected the *E* isomer is 12.2 kJ/mol more stable than the *Z* isomer. The irradiation of **1-*E*** with a 250 Watts mercury lamp produced the *Z* isomer, which was isolated by column chromatography in a 67% yield.

For **1-*Z***, the ^{1}H-NMR spectra show the existence of an intramolecular H-bond after irradiation with UV light since all the signals changed their chemical shift. The lack of symmetry in the molecule is reflected by the different coupling between the signals and the shift of the N-*H* proton in **1-*Z*** when compared to **1-*E*** (See Figure 2). The most remarkable change occurs on the NH and phenyl protons, which are shifted to the up-field region and splitted as a multiplet, respectively.

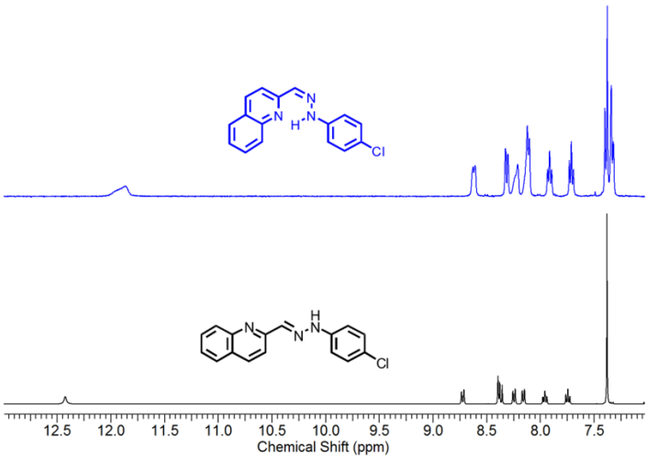

Figure 2.^{1}H NMR spectra (400 MHz) of compound **1-*E*** and **1-*Z*** in DMSO-d_6.

Single-crystal structure determination

Crystals of **1-*E*** were obtained by slow evaporation of ethanol, resulting in fine, orange needlelike crystals. **1-*E*** crystalized in the monoclinic space group P21/c. The molecule presents an almost planar configuration with a torsion angle between C_6–C_1–N_1– N_2 of 5.89(1)° and a dihedral angle between the quinoline and benzene planes of 1.91°. The Mogul geometry check shows that all bond lengths and angles are within the normal range *(28)*. ORTEP representation of the **1-*E*** structure is presented in the Figure 3a; Crystal data collection and structure refinement details are summarized in Table 1.

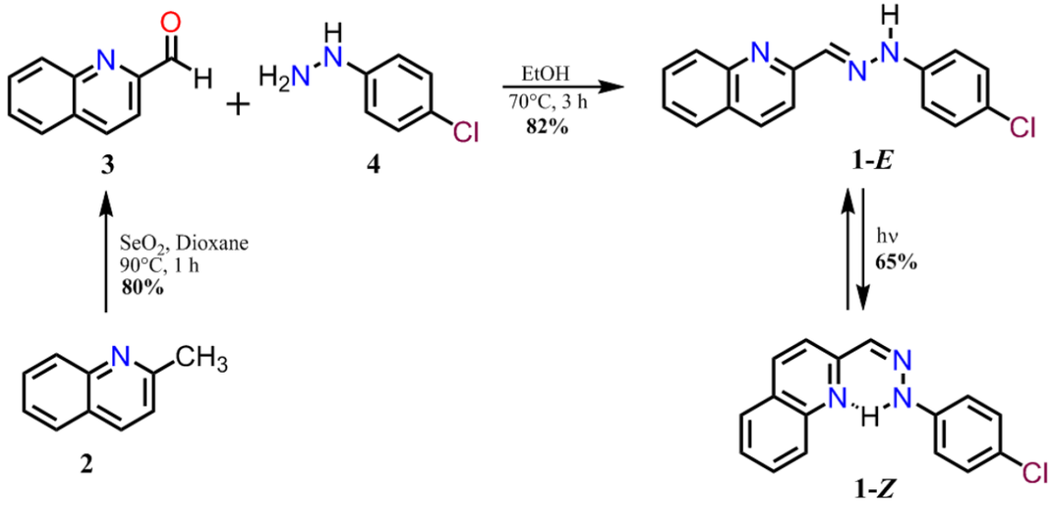

Figure 1. Synthetic route to obtain the hydrazone derivative **1**.

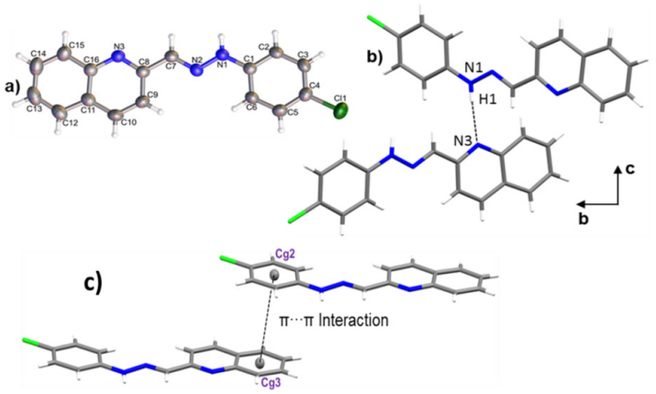

Figure 3. a) ORTEP representation of title compound, b) Hydrogen bond N1–H1···N3 and c) a) π···π interaction between Cg2 and Cg3.

The crystal packing is driven by N_1–H_1···N_3 hydrogen bond, along [010] direction with 3.0855(1) Å of distance. As shown in Figure 3b, the interactions give rise to zig-zag chains growing along the [010] direction and the connected molecules are placed on the two planes (931) and (12-41). A 3D supramolecular network is formed by the joining of the chains along [100] direction by π-π interactions between the aromatic rings with an intercentroids distance of Cg2···Cg3= 3.8903(1) Å (Figure 3 c). It was also observed a C_9–H_9 ···C_{11} interaction *(29)* along [001] direction with a distance of 3.7168(15) Å.

The Hirshfeld surface for **1-*E*** showed that the chloride and the deprotonated nitrogen atoms in the quinoline and hydrazone present mainly, a hydrogen acceptor behavior, while the N–H and C–H act as donor groups (see Figure 4). Furthermore, an observation over the aromatic rings in the shape index surface blue and red regions that indicates the presence of π-π interactions, is confirmed by the fingerprint plot. The greatest contribution comes from Van der Waals interactions (H···H and C···H) followed by hydrogen bonds as C l ···H and N···H (see Figure 4b), that contribute with 15.6% and 7.9%, respectively. The π-π interactions contribute with 10.9% . Other contacts were also observed, however, their contribution is less than 5% each.

Molecular geometry optimization

Ab initio calculations yielded a planar structure with a dihedral angle equals to 0.001º between the quinoline and benzene planes and ~0º torsion angles between the quinoline or benzene rings and the hydrazine group. As shown in Figure 5, these dihedral and torsional angles are not significantly deviated concerning to the results discussed in the crystallographic section.

Linear regression analysis was also carried out to establish a systematic comparison between the optimized and crystallographic structures. The slope represents a ratio between the set of variations of calculated-experimental data. The intercept corresponds to the value of the dependent variable (calculated) when the independent variable (experimental) is equal to zero: meaning an over or underestimation value. Thus, perfect correlation is given when the slope and intercept values are 1 and 0, respectively (selected structural parameters and linear regression are shown in Table 2). The analysis reveals that theoretical calculations tend to a subtle overestimation respect to the crystallographic data set as shown in the intercept values (see Table 2).

Table 1. Crystal data and structure refinement for **1-*E***.

Identification Code	1-*E*
Empirical formula	$C_{16}H_{11}ClN_3$
Formula weight	280.73
Temperature/K	296(2) K
Crystal system	Monoclinic
Space group	$P_{21/c}$
a/Å	8.2023(3)
b/Å	7.1828(2)
c/Å	23.2593(8)
β(°)	90.5180(10)
Volume/ Å^3	1370.28(8)
Z	4
ρ_{calc} mg/ mm^3	1.361
μ/mm^{-1}	0.271
F(000)	580
Crystal size/ mm^3	0.522 x 0.178 x 0.171
2θ range for data collection/°	1.751 to 26.412
Index ranges	-10≤h≤10, -8≤k≤8, -29≤l≤29
Reflections collected	38252
Independent reflections	2810[R(int) = 0.0241]
Data / restraints / parameters	2810 / 0 / 185
Goodness-of-fit on F^2	1.050
Final R indices [I>2sigma(I)]	R1 = 0.0371, wR2 = 0.0999
R indices (all data)	R1 = 0.0442, wR2 = 0.1067
Largest diff. Peak/hole/ e.Å^{-3}	0.204 and -0.209

The highest deviation from experimental bond length measurements was observed in N_1–H bond (17.17% error) since this group is highly influenced by hydrogen bond interaction (See Figure 3). However, other bond angles and length show less than 1.4% and 0.9% bond length and angle errors respectively.

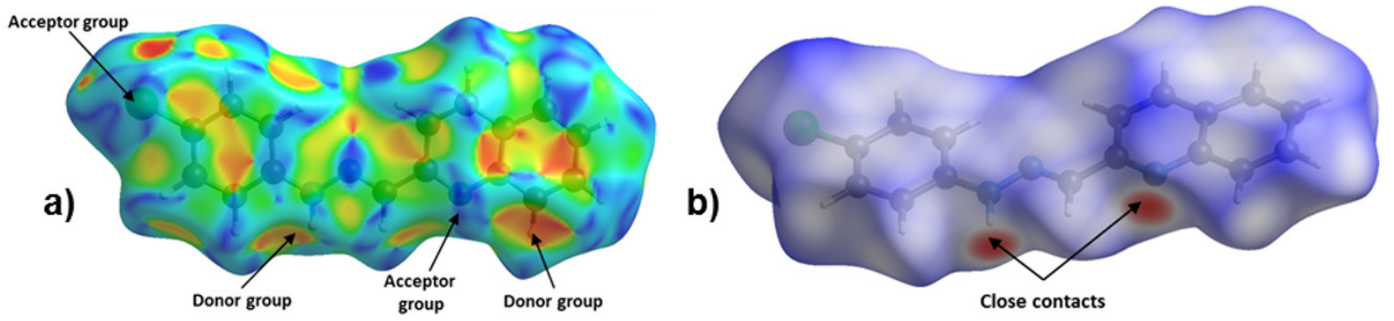

Figure 4. Hirshfeld Surface of title compound. Left: a) Shape Index and Right: b) dnorm.

UV-Vis Spectroscopy analysis

The electronic transitions of **1-*E*** were studied by UV-Vis. As shown in Figure 6, the hydrazone derivative exhibits a high absorption band around 425 nm, which present a bathochromic shift with the increasing polarity of the solvent. Additionally, a new band around 380 nm corresponding to π-π* transitions related to the imine bond was observed using methanol as solvent *(6)*. An optimized structure by DFT: B3LYP/6-311+G (d, p) calculation was used as input geometry for a second optimization at HF/6-31+G (d) level of theory including solvent effects through the SCI-PCM approximation to simulate chloroform solvation yielding an equivalent conformation with no differences in the electronic structure. From this optimized structure, TD-SCF method was employed to calculate excited states energy at HF/6-31+G (d) level of theory neglecting solvation. Besides, the theoretical UV-Visible spectrum presents a transition in the visible region and two transitions in the ultraviolet region (absorptions at 427, 319, and 278 nm respectively) with an absolute error percentage respect to experimental observations equal to 6.57, 10.34, and 11.15%, respectively. These results tend to an underestimation in a range between 28 to 33 nm.

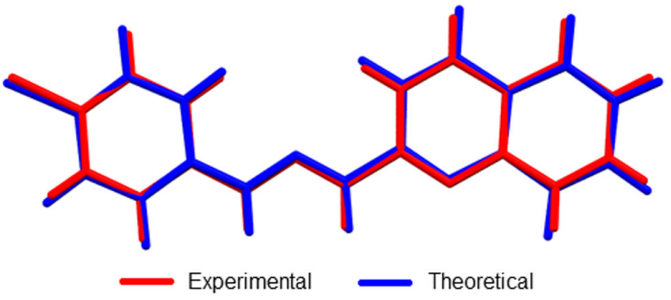

Figure 5. Overlap of crystallographic and optimized (DFT: B3LYP/6-311+G (d, p) structures of **1-*E***. RMSD was 0.0985.

GaussSum 3.0 software package was employed to deconvolute the computed electronic transitions using Gaussian 09 and to determine the contribution of the main electronic transitions (see Figure 7). Higher oscillator strength was observed at 427 nm signal (0.3465). This absorption maximum was characterized by a main electronic transition from HOMO to LUMO+1 energy levels (34%), where a homogeneous electronic distribution is displaced to a MO over the hydrazone and phenyl groups.

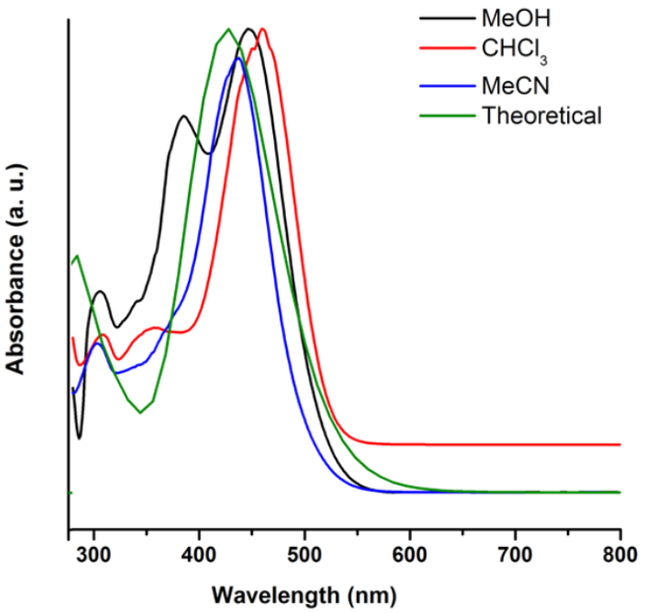

Figure 6. Theoretical and experimental UV-vis spectra of **1-*E*** (1.0 x 10^{-5} M) in different solvents.

A second main electronic transition from HOMO-2 to LUMO+1 (5%) was also observed. Second higher oscillator strength was observed at 278 nm (0.1705), where the main electronic transition (HOMO-1→LUMO+5, 21%) is characterized by a partial electronic displacement from the quinoline to hydrazone and chlorophenyl moieties.

NMR and FT-IR spectroscopy analysis

Theoretical-experimental comparison of FT-IR and NMR spectra of **1-*E*** was also carried out. The four most prominent bands are C=N stretching (1579 cm^{-1}), N-H rocking (1508 cm^{-1}), N-N stretching (1142 cm^{-1}), and C-H bending (1241cm^{-1}). Displacement vectors for these vibrations are shown in Figure 8.

Table 2. Theoretical-experimental comparison of selected molecular geometry parameters.

Bond	Experimental length (Å)	Calculated length (Å)	Error (%)
C_1-C_2	1,388	1.4020	1.01
C_2-C_3	1.377	1.3897	0.92
C_3-C_4	1.378	1.3912	0.96
C_4-C_1	1.742	1.7605	1.06
C_4-C_5	1.391	1.3914	1.12
C_5-C_6	1.380	1.3904	0.75
C_6-C_1	1.391	1.4009	0.71
C_1-N_1	1.388	1.3938	0.42
N_1-H*	0.867	1.0159	17.17
N_1-N_2	1.348	1.3388	0.68
N_2-C_7	1.279	1.2859	0.54
C_7-C_8	1.456	1.4622	0.43
C_8-N_3	1.323	1.3240	0.08
C_8-C_9	1.42	1.4266	0.46
C_9-C_{10}	1.352	1.3664	1.07
C_{10}-C_{11}	1.414	1.4202	0.44
C_{11}-C_{16}	1.417	1.4293	0.87
C_{11}-C_{12}	1.410	1.4155	0.39
C_{12}-C_{13}	1.359	1.3763	1.27
C_{13}-C_{14}	1.395	1.4144	1.39
C_{14}-C_{15}	1.366	1.3753	0.68
C_{15}-C_{16}	1.408	1.4186	0.75
C_{16}-N_3	1.372	1.3610	0.80
Linear regression			
Slope		1.0300	
Intercept		0.0337	
R^2		0.99301	
Bond	**Crystallographic angle (º)**	**Calculated angle (º)**	**Error (%)**
C_3-C_4-C_5	120.51	120.49	0.02
C_5-C_4-C_1	119.62	119.79	0.14
C_6-C_1-N_1	121.84	121.95	0.09
N_1-N_2-C_7	117.53	118.28	0.64
C_7-C_8-N_3	116.41	115.38	0.89
C_9-C_{10}-C_{11}	120.33	119.85	0.40
C_{11}-C_{12}-C_{13}	120.72	120.47	0.20
C_{14}-C_{15}-C_{16}	120.46	120.44	0.02
C_{16}-N_3-C_8	118.19	118.68	0.42
Linear regression			
Slope		1.0242	
Intercept		2.9178	
R^2		0.9223	

* Bond length linear regression exclude N_1-H bond

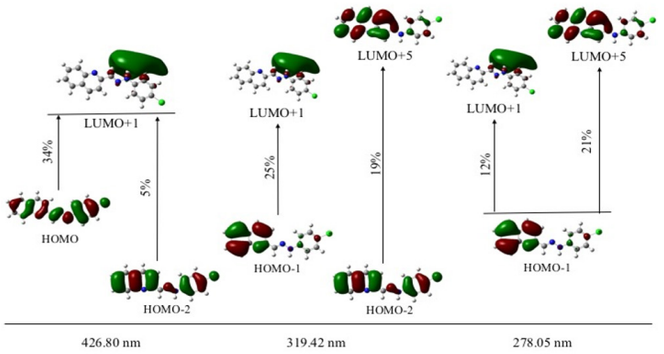

Figure 7. Main electronic transitions in ultraviolet-visible and contribution percentage.

These vibrational modes are degenerated except *N*-H bending since displacement vectors clearly showed other vibrational modes coexisting simultaneously in each frequency.

The absence of imaginary frequencies confirms that the optimized structure is a global minimum. A comparison of selected computed vibrational frequencies and assigned values experimentally is shown in Table 3 from supporting information. Calculated values tend to overestimation even though the scale factor used is less than 1.00 *(30)*. The maximum error rate was observed in C-Cl frequency (5.45%), C=N and N-H frequencies are the second and third biggest deviation respect to experimental observations. C-Cl and N-H errors may be explained because these moieties are typically involved in hydrogen bonding interactions in the solid state and those were neglected in theoretical calculations.

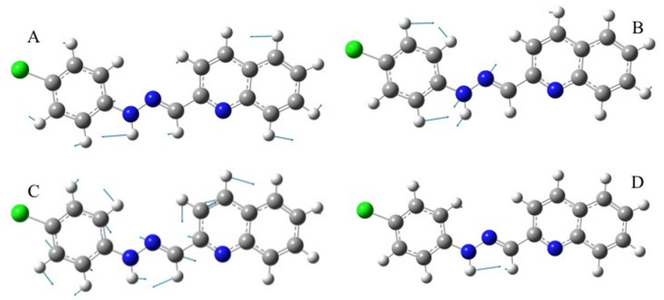

Figure 8. Displacement vectors for selected vibrational modes. A) C-H bending. B) N-N stretching. C) C=N stretching. D) N-H bending.

The correlation between the computed and experimental ^{1}H-NMR chemical shifts was unacceptable as the signal of *N*-H, showed the biggest deviation (see Table 4), mainly due to its high influence by solvation *(31)*. Therefore, the neglected solvation effect should help to improve the quality of ^{1}H-NMR chemical shift calculations. The ^{13}C-NMR chemical shifts showed acceptable correlation respect to experimental values yielding an average rate of error equal to 2.61%.

Electrochemical studies

The electrochemical properties of compounds **1-*E*** and **1-*Z*** were studied by cyclic voltammetry (CV) and Osteryoung Square Wave Voltammetry (OSWV) (See Materials and Methods Section).

Table 3. Theoretical-Experimental comparison of vibrational frequencies.

Vibrational mode	Theoretical (cm^{-1})	Scaled value (cm^{-1})	Experimental frequency (cm^{-1})	Error rate (%)
N-H stretching	3499	3387	3209	5,26
N=C-H stretching	3062	2964	2985	-0,71
C=N stretching	1631	1579	1495	5,32
N-N stretching	1180	1142	1091	4,47
C-Cl stretching	1100	1065	1007	5,45
C=C stretch. Aryl	1640	1587	1587	0.02
N-H rocking	1558	1508	1555	-3,12
C-H bending	1282	1241	1236	0,40

When analyzing the cathodic potentials (see Figure 9), three irreversible reduction potentials for the ***1-E*** isomer are observed. These potentials remained irreversible upon increasing scan rates. OSWV revealed two additional reductions (see Figure 10) which are located very close to those observed in CV. Presumably, the closed peak potentials correspond to the processes occurring on the surface of the electrode and the corresponding cathodically shifted potential to the process occurring in the solution. The first reduction in compound ***1-E*** is located at -1.09 V and corresponds to the imine reduction whereas for ***1-Z*** is cathodically shifted towards -2.54 V (see Table 5). These results indicate that upon reduction the [**1-E**]$^{\cdot -}$ radical anion is stabilized by π delocalization in the quinoline system. However, in the *Z* configuration the nitrogen from the quinoline is acting as a Lewis base (forming the intramolecular hydrogen bond) and, therefore, its participation in the radical anion stabilization is restricted thus shifting cathodically the reduction potential. Likewise, the differences in the current intensity for the cathodic/anodic potentials suggest different reduction mechanism for both configurational isomers.

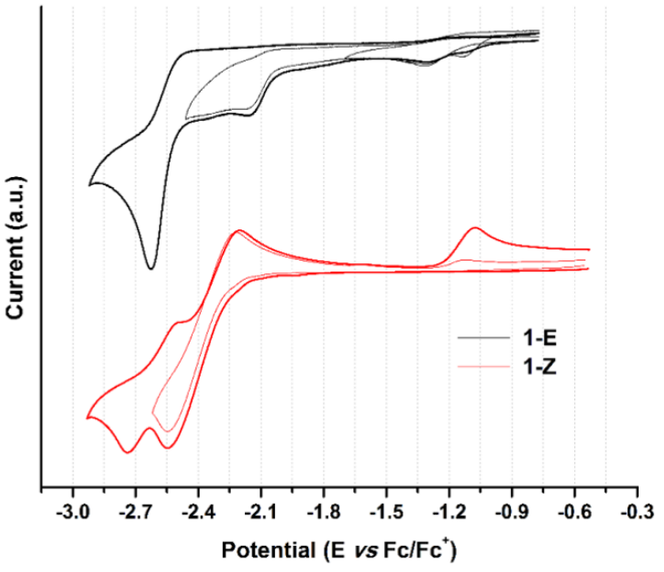

Figure 9. Cyclic voltammogram of hydrazone configurational isomers at 100 mVs^{-1}. Glassy carbon as working electrode and ferrocene as an internal reference.

Table 4. Theoretical-experimental comparison of vibrational frequencies.

^{1}H-NMR Chemical shift (ppm)			^{13}C-NMR Chemical shift (ppm)		
Experimental	**Calculated**	**Error**	**Experimental**	**Calculated**	**Error**
7.38	7.00	-5.43	115.8	113.81	1.72
7.38	7.73	4.53	118.4	114.54	3.26
7.38	7.94	7.05	122.6	129.09	-5.29
7.38	8.26	10.65	125.9	129.41	-2.79
7.75	8.10	4.32	126.6	130.46	-3.05
7.97	8.35	4.55	127.4	131.88	-3.52
8.16	8.25	1.09	128.4	132.08	-2.87
8.25	8.55	3.51	128.8	134.87	-4.71
8.35	8.82	5.33	129.1	137.89	-6.81
8.72	8.71	-0.11	129.7	136.57	-5.30
12.43	7.47	-66.40	133.2	138.54	-4.01
-	-	-	142.03	139.14	2.03

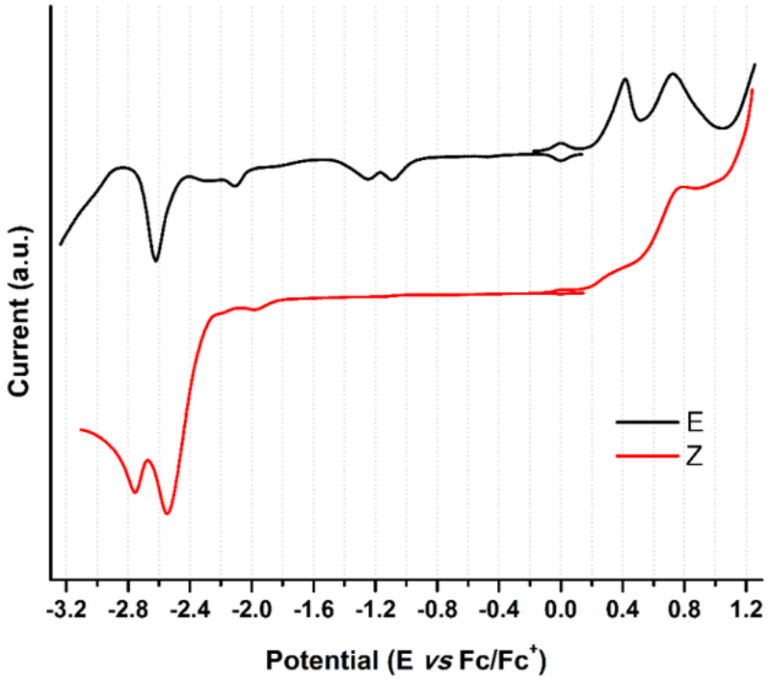

Figure 10. OSW of hydrazone derivatives **1-*E*** and **1-*Z*** at 100 mVs-1. Glassy carbon as working electrode and using ferrocene as an internal reference.

Table 5. Electrochemical ootentials of hydrazone derivatives *vs* ferrocene in DMF (V)[a].

Compound	$E_{p, oxd(1)}$	$E_{p, oxd(2)}$	$E_{p, red(1)}$	$E_{p, red(2)}$	$E_{p, red(3)}$	$E_{p, red(4)}$	$E_{p, red(5)}$
1-*E*	0.42	0.73	-1.09	-1.24	-2.10	-2.28	-2.62
1-*Z*	0.31	0.76	-2.54	-2.75			

[a]Working electrode: glassy carbon; counter electrode: Pt wire; Pseudoreference electrode: Ag wire. Supporting electrolyte: $TBAPF_6$.Scan rate: 0.1 V s^{-1}.

Compounds ***1-E*** and ***1-Z*** exhibited two irreversible oxidation potentials which are attributed to the –NH groups of the hydrazone framework. The first reduction potential of ***1-E*** is anodically shifted, when compared to its ***1-Z*** counterpart. This behavior indicates a larger acidity of **1-Z** gained by the intramolecular hydrogen bond formation.

Conclusions

The solid-state structural investigation trough single-crystal X-ray diffraction reveals a crystal packaging governed by N_1–$H_1\cdots N_3$ hydrogen bond, forming inverted dimers along [010] direction. The theoretical calculations carried out at DFT: B3LYP/6-311+G (d, p) level of theory showed good correlation with experimental data, yielding error rates less than 1.4% and 0.9% error for bond lengths and angles. Also, spectroscopic properties were successfully calculated employing *ab initio* calculations. The UV-Vis spectrum was deconvoluted giving the main electronic transitions from HOMO to LUMO+1 and HOMO-1 to LUMO+5.

In solution, this novel compound exhibited UV radiation-mediated configurational isomerism conversion from **1-*E*** to **1-*Z*** confirmed by ^{1}H-NMR evidence: chemical shift change and new signals appearance owing to system asymmetry. Finally, modified electrochemical behavior induced by configurational changes was observed, supporting the applicability of these type of molecular systems as an electrochemical template.

Acknowledgements

The authors are grateful to the Vicerrectoria de Investigaciones and Centro de Excelencia en Nuevos Materiales (CENM) from the Universidad del Valle (Colombia), as well as the Departamento Administrativo de Ciencia, Tecnología e Innovación (COLCIENCIAS) for the financial support of this work. M.S.-M. and R. D. acknowledges Coordenação de Aperfeiçoamento de Pessoal de Nível Superior and Conselho Nacional de Desenvolvimento Cientfico y Tecnológico for the CNPq and CAPES/PNPD scholarships from Brazilian Ministry of Education, and R. de Almeida Santos to facilitate the measurements and FAPESP (2009/54011-8) for providing Apex-II equipment. R.F.D. acknowledges to the Dirección General de Investigaciones (DGI) of the Universidad Santiago de Cali. G.G. thanks to the Laboratorio de Computación Científica from Facultad de Ciencias Naturales (Icesi University) for the computational resources support as well as Prof. Carlos A. Arango for his invaluable guidance.

References

1. Lehn, J.-M. Perspectives in Chemistry—Aspects of Adaptive Chemistry and Materials. *Angew. Chemie Int. Ed*. **2015**, *54* (11), 3276–3289. DOI: https://doi.org/10.1002/anie.201409399.
2. Li, J.; Nowak, P.; Otto, S. Dynamic Combinatorial Libraries: From Exploring Molecular Recognition to Systems Chemistry. *J. Am. Chem. Soc*. **2013**, *135* (25), 9222–9239. DOI: https://doi.org/10.1021/ja402586c.
3. Tatum, L. A.; Su, X.; Aprahamian, I. Simple Hydrazone Building Blocks for Complicated Functional Materials. *Acc. Chem. Res*. **2014**, 47 (7), 2141–2149. DOI: https://doi.org/10.1021/ar500111f.
4. Su, X.; Aprahamian, I. Hydrazone-Based Switches, Metallo-Assemblies and Sensors. *Chem. Soc. Rev*. **2014**, *43* (6), 1963–1981. DOI: https://doi.org/10.1039/C3CS60385G.
5. Lehn, J.-M. Conjecture: Imines as Unidirectional Photodriven Molecular Motors -Motional and Constitutional Dynamic Devices. *Chemistry*. **2006**, *12* (23), 5910–5915. DOI: https://doi.org/10.1002/chem.200600489.
6. Chaur, M. N.; Collado, D.; Lehn, J.-M. Configurational and Constitutional Information Storage: Multiple Dynamics in Systems Based on Pyridyl and Acyl Hydrazones. *Chem. A Eur. J*. **2011**, *17* (1), 248–258. DOI: https://doi.org/10.1002/chem.201002308.
7. Romero, E. L.; D´Vries, R. F.; Zuluaga, F.; Chaur, M. N. Multiple Dynamics of Hydrazone Based Compounds. *J. Brazilian Chem. Soc*. **2015**, *26* (6), 1265–1273. DOI: http://dx.doi.org/10.5935/0103-5053.20150092.
8. Gordillo, M. A.; Soto-Monsalve, M.; Gutiérrez, G.; D'Vries, R. F.; Chaur, M. N. Theoretical and Experimental Comparative Study of a Derivative from 2-Pyridinecarboxaldehyde Which Exhibits Configurational Dynamics. *J. Mol. Struct*. **2016**, *1119*. DOI: https://doi.org/10.1016/j.molstruc.2016.04.055.
9. Chaur, M. N. Aroylhydrazones as potential systems for information storage: photoisomerization and metal complexation *Rev. Colomb. Quim*. **2012**, *41* (3), 349-358.
10. Ulrich, S.; Buhler, E.; Lehn, J.-M. Reversible Constitutional Switching between Macrocycles and Polymers Induced by Shape Change in a Dynamic Covalent System. *New J. Chem*. **2009**, *33* (2), 271–292. DOI: https://doi.org/ 10.1039/B817261G.
11. Carmona-Vargas, C. C.; Váquiro, I. Y.; Jaramillo-Gómez, L. M.; Lehn, J.-M.; Chaur, M. N. Grid-Type Complexes of M2+ (M=Co, Ni, and Zn) with Highly Soluble Bis(hydrazone)thiopyrimidine-Based Ligands: Spectroscopy and Electrochemical Properties. *Inorganica Chim. Acta*. **2017,** *468*, 131–139. DOI: https://doi.org/10.1016/j.ica.2017.05.002.
12. Su, X.; Robbins, T. F.; Aprahamian, I. Switching through Coordination-Coupled Proton Transfer. *Angew. Chemie Int. Ed*. **2011**, *50* (8), 1841–1844. DOI: https://doi.org/ 10.1002/anie.201006982.
13. Romero, E. L.; Cabrera-Espinoza, A.; Ortiz-Peña, N.; Soto-Monsalve, M.; Zuluaga, F.; D'Vries, R. F.; Chaur, M. N. New Pyrazolino and pyrrolidino[60]fullerenes: The Introduction of the Hydrazone Moiety for the Formation of Metal Complexes. *J. Phys. Org. Chem*. **2017**, *30* (2), e3601–n/a. DOI: https://doi.org/10.1002/poc.3601.
14. Gutiérrez, G; Gordillo, M.A.;Chaur, M. N. A DFT study on Dichloro {(E)-4-dimethylamino-N'-[(pyridin-2-yl) methylideneKN] benzohydrazide-k0}M2+ (M = Zn, Cu, Ni, Fe, Mn, Ca and Co) complexes: Effect of the metal over association energy and complex geometry. *Rev. Colomb. Quim*. **2016**, *45* (3) 28-32. DOI: https://doi.org/10.15446/rev.colomb.quim.v45n3.57351.
15. Landge, S. M.; Tkatchouk, E.; Benítez, D.; Lanfranchi, D. A.; Elhabiri, M.; Goddard, W. A.; Aprahamian, I. Isomerization Mechanism in Hydrazone-Based Rotary Switches: Lateral Shift, Rotation, or Tautomerization? *J. Am. Chem. Soc*. **2011**, *133* (25), 9812–9823. DOI: https://doi.org/10.1021/ja200699v.
16. Castro Agudelo, B.; Ochoa-Puentes, C.; Rodríguez-Córdoba, W.; Reiber, A.; Sierra, C. A. Synthesis, characterization, X-ray crystal structure and DFT calculations of 4-([2,2':6',2"-terpyridin]-4'-yl) phenol *Rev. Colomb. Quím*. **2018**, *47* (1). In press. DOI: https://doi.org/10.15446/rev.colomb.quim.v47n1.66281.
17. Parada, G.; Fernández, D.; Reyes, A.; Suárez, M.F.; Fadini, L. Sinteis y Estudio Teorico de Compuesto de Ru(II) con Ligantes Ferrocennílicos para Aplicaciones Electroquímicas. *Rev. Colomb. Quim*. **2007**, *36* (2), 199-211.
18. Fernández, M. A.; Barona, J. C.; Polo-Cerón, D.; Chaur, M. N. Photochemical and Electrochemical Studies on Lanthanide Complexes of 6-(Hydroxymethyl)pyridine- 2-carboxaldehyde[2- Methyl-Pyrimidine-4,6-Diyl] Bis-Hydrazone. *Rev. Colomb. Quím*. **2014**, *43* (1), 5–11. DOI: https://doi.org/10.15446/rev.colomb.quim.v43n1.50540.

19. Puskullu, M. O.; Shirinzadeh, H.: Nenni, M.; Gurer-Orhan, H.; Suzen, S. Synthesis and evaluation of antioxidant activity of new quinoline-2-carbaldehyde hydrazone derivatives: bioisosteric melatonin analogues. *J. Enzyme Inhib. Med. Chem.* **2016,** *31* (1): 121–125. DOI: https://doi.org/10.3109/14756366.2015.1005012.
20. Bruker-AXS. SAINT. Bruker-Siemens: Madison, Wisconsin,USA 2006.
21. Sheldrick, G. M. Crystal Structure Refinement with SHELXL. *Acta Crystallogr. Sect. C Struct. Chem.* **2015**, *71* (1), 3–8. DOI: https://doi.org/10.1107/S2053229614024218.
22. Farrugia, L. J. WinGX and ORTEP for Windows : An Update. *J. Appl. Crystallogr*. **2012**, *45* (4), 849–854. DOI: https://doi.org/10.1107/S0021889812029111.
23. Dolomanov, O. V.; Bourhis, L. J.; Gildea, R. J.; Howard, J. A. K.; Puschmann, H. OLEX2 : A Complete Structure Solution, Refinement and Analysis Program. *J. Appl. Crystallogr.* **2009**, *42* (2), 339–341. DOI: https://doi.org/10.1107/S0021889808042726.
24. Macrae, C. F.; Bruno, I. J.; Chisholm, J. A.; Edgington, P. R.; McCabe, P.; Pidcock, E.; Rodriguez-Monge, L.; Taylor, R.; van de Streek, J.; Wood, P. A. Mercury CSD 2.0 – New Features for the Visualization and Investigation of Crystal Structures. *J. Appl. Crystallogr*. **2008**, *41* (2), 466–470. DOI: https://doi.org/10.1107/S0021889807067908.
25. Dennington, R.; Keith, T.; Millam, J. GaussView. Semichem Inc.: Shawnee Mission 2009.
26. Frisch, M. J.; Trucks, G. W.; Schlegel, H. B.; Scuseria, G. E.; Robb, M. A.; Cheeseman, J. R.; Scalmani, G.; Barone, V.; Mennucci, B.; Petersson, G. A.; et al. Gaussian 09. Gaussian, Inc.: Wallingford CT 2009.
27. O'Boyle, N. M.; Tenderholt, A. L.; Langner, K. M. Cclib: A Library for Package-Independent Computational Chemistry Algorithms. *J. Comput. Chem.* **2008**, *29* (5), 839–845. DOI: https://doi.org/ 10.1002/jcc.20823.
28. Bruno, I. J.; Cole, J. C.; Kessler, M.; Luo, J.; Motherwell, W. D. S.; Purkis, L. H.; Smith, B. R.; Taylor, R.; Cooper, R. I.; Harris, S. E.; et al. Retrieval of Crystallographically-Derived Molecular Geometry Information. *J. Chem. Inf. Comput. Sci*. **2004**, *44* (6), 2133–2144. DOI: https://doi.org/10.1021/ci049780b.
29. B. Aakeroy, C.; A. Evans, T.; R. Seddon, K.; Palinko, I. The C-H···Cl Hydrogen Bond: Does It Exist? *New J. Chem.* **1999**, *23* (2), 145–152. DOI: https://doi.org/10.1039/A809309A.
30. Andersson, M. P.; Uvdal, P. New Scale Factors for Harmonic Vibrational Frequencies Using the B3LYP Density Functional Method with the Triple-ζ Basis Set 6-311+G(d,p). *J. Phys. Chem. A*. **2005**, *109* (12), 2937–2941. DOI: https://doi.org/10.1021/jp045733a.
31. Friebolin, H. Basic One-and Two-Dimensional NMR Spectroscopy; John Wiley & Sons, Inc: Weinheim, 1993.

Article citation:
Romero, E. L.; Soto-Monsalve, M.; Gutiérrez, G.; Zuluaga, F.; D´Vries, R.; Chaur, M. N. Structural, spectroscopic, and theoretical analysis of a molecular system based on 2-((2-(4-chlorophenylhydrazone)methyl)quinolone. *Rev. Colomb. Quim.* **2018,** *47* (2), 63-72. DOI: https://doi.org/10.15446/rev.colomb.quim.v47n2.67115.